

System for detecting acoustic emissions in multianvil experiments: Application to deep seismicity in the Earth

Haemyeong Jung^{a)}

Institute of Geophysics and Planetary Physics, University of California, Riverside, California 92521; Geophysical Laboratory, Carnegie Institute of Washington, Washington, DC 20015 and Department of Terrestrial Magnetism, Carnegie Institute of Washington, Washington, DC 20015

Yingwei Fei

Geophysical Laboratory, Carnegie Institute of Washington, Washington, DC 20015

Paul G. Silver

Department of Terrestrial Magnetism, Carnegie Institute of Washington, Washington, DC 20015

Harry W. Green

Institute of Geophysics and Planetary Physics, University of California, Riverside, California 92521 and Department of Earth Sciences, University of California, Riverside, California 92521

(Received 15 June 2005; accepted 3 November 2005; published online 12 January 2006)

One of the major goals in the experimental study of deep earthquakes is to identify slip instabilities at high pressure and high temperature (HPHT) that might be responsible for the occurrence of earthquakes. Detecting acoustic emissions from a specimen during faulting provides unique constraints on the instability process. There are few experimental studies reporting acoustic emissions under HPHT conditions, due to technical challenges. And those studies have used only one or at most two acoustic sensors during the experiments. Such techniques preclude the accurate location of the acoustic emission source region and thus the ability to distinguish real signal from noise that may be coming from outside the sample. We have developed a system for detecting acoustic emissions at HPHT. Here we present a four-channel acoustic emission detecting system working in the HPHT octahedral multianvil apparatus. Each channel has high resolution (12 bits) and a sampling rate of 30 MHz. In experiments at the pressures up to 6 GPa and temperatures up to 770 °C, we have observed acoustic emissions under various conditions. Analyzing these signals, we are able to show that this system permits us to distinguish between signal and noise, locate the source of the acoustic emission, and obtain reliable data on the radiation pattern. This system has greatly improved our ability to study faulting instabilities under high pressure and high temperature. © 2006 American Institute of Physics. [DOI: 10.1063/1.2148994]

I. INTRODUCTION

Mechanisms of intermediate (~50–300 km) and deep (>300 km) earthquakes have been investigated in laboratory experiments under high pressure and high temperature.^{1–9} Both intermediate and deep earthquakes constitute the sudden release of the elastic energy in a shear pattern under high pressure and high temperature^{10–15} and thus appear in many ways like that shallow that are well explained by brittle failure. This same mechanism, however, is difficult to explain at high confining pressures, so that the physical mechanism of these deeper events has not been equally well explained. Therefore, detecting acoustic emissions (AE) during a high pressure faulting experiment can provide us with unique and very important information to understand the mechanism of these deep earthquakes. Several authors recently reported AE at high pressure and high temperature

under the dehydration of serpentine,^{4–6} or under the solid-solid phase transformation.^{3,16} These experimental observations have supported both dehydration embrittlement of hydrous minerals and solid-solid phase transformation as possible explanations for the occurrence of deep earthquakes. However, all the previous studies used only one or two channels in acoustic emission detection. Even when wave forms were recorded, no information was available on the radiation pattern of those events. In other words, it is not clear from the AE alone whether those events were processes of shear, explosion, or implosion. Furthermore, with one or two channels it is very difficult to distinguish between real events and noises. In this study, we report an improved system for studying acoustic emissions under high pressure and high temperature.

The major requirements for the system are that it must work with proper high-*PT* experimental systems above several GPa and several hundred degrees; it must be a multi-channel, digital wave form recording system with a sampling rate as high as possible up to the order of 10 MHz, resolution as high as possible up to 16 bits, and dead time as short as possible. None of the existing systems could meet these re-

^{a)} Author to whom correspondence should be addressed; current address: School of Earth and Environmental Sciences, Seoul National University, San 56-1 Sillim-dong, Gwanak-gu, Seoul 151-747, Korea; electronic mail: hjung@ucr.edu

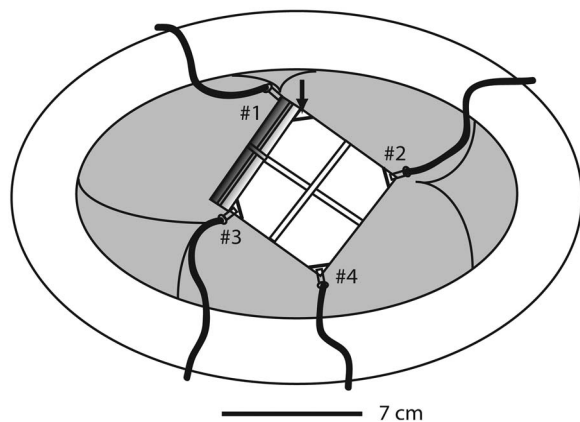


FIG. 1. Position of four transducers in the multi-anvil box. Four acoustic sensors (1–4) are attached to the outer truncated edges of the tungsten carbide (WC) cubes. The upper most truncated edge is shown by arrow. Cables carrying acoustic signals are shown as thick lines.

quirements to a satisfactory level. All previous systems working in high-pressure and high-temperature experiments had relatively low spatial resolution. For systems working at low pressure and room temperature, the best system reported in the literature, to our knowledge, is the one described by Lei *et al.*,^{17,18} with 20 MHz sampling rate, 12-bit resolution, 0.3 s dead time, and 60 MPa confining pressure. In this study, we implemented a multichannel digital wave form recording system with 30 MHz sampling rate, 12-bit resolution, 0.4 s dead time that works in an octahedral multi-anvil apparatus with pressures and temperatures up to $P=9$ GPa and $T=1000$ °C (extendable to $P=27$ GPa with smaller truncated edge length and smaller sample size and temperatures up to $T=2400$ °C). In this article we describe the system and then show results from calibration experiments which demonstrate the improvements of this system in detecting acoustic emission in high-pressure and high-temperature experiments.

II. EXPERIMENTAL SYSTEM

A. Apparatus and acoustic sensor positions

The mechanical system to generate high pressure is a multi-anvil apparatus (Prensall Press), installed at the Geophysical Laboratory of the Carnegie Institution of Washington. The apparatus can be used to generate high pressures up to ~ 27 GPa and high temperatures up to ~ 2400 °C using small sample assemblies. It consists of six push wedges (three on the top pressure ram and the other three on the bottom ram). The wedges transmit the uniaxial compressive force of the hydraulic ram onto the faces of a cube that is assembled from eight separate tungsten carbide (WC) cubes. Four acoustic sensors (piezoelectric transducers described in the next section), were attached to the outer truncated edges of the WC cubes, as shown in Fig. 1. Cables carrying the signals are guided to the amplifier inside the data acquisition box through the spaces between the top and bottom pressure rams (Fig. 2). There are a total of eight outer truncated corners on the eight WC cubes when the sample assembly is placed in the apparatus. The uppermost (shown by the arrow in Fig. 1) and the lower-most truncated corners are used as

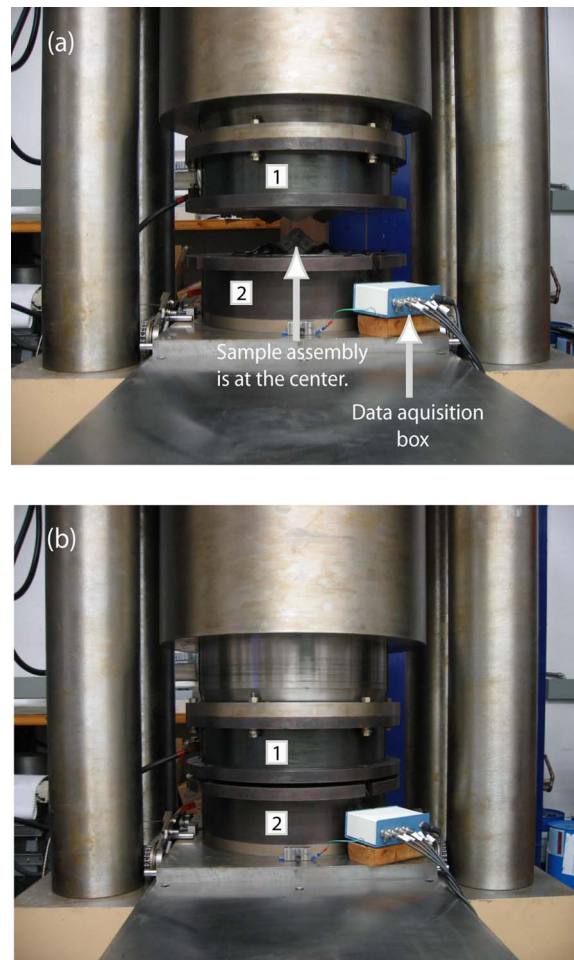


FIG. 2. (Color online) A multi-anvil apparatus (Prensall press) (1) Top pressure ram (2) Bottom pressure ram. (a) Loaded sample at room pressure. Sample assembly is located at the center. (b) Pressurized sample to $P=6$ GPa.

an electric leads for the furnace. Among the other six truncated corners, three of them are in the upper half of the assembly while the other three are in the lower half. In our experiments, transducers 1–3, are located in the upper half while transducer 4 is in the lower half (Fig. 1). The location of the four transducers is symmetric with respect to the center of the sample assembly. Therefore, for events which occur in the central area (where the sample is), the arrival time of waves should be the same for the four channels. On the other hand, the further an event is from the center, the larger will be the differences in the arrival time of the waves recorded on different channels. This configuration of four channels constrains the source location of acoustic emission, as shown below, as well as providing an excellent constraint on the radiation pattern.

B. Acoustic sensors (transducers) and data collecting system

Transducers attached to the anvils' truncated corners require that the transducers have high sensitivity and high Curie temperature. For the experiments of ~ 1000 – 1800 °C, the temperature on the outer truncated corners of the WC cubes is ~ 200 – 300 °C, which is about the Curie tempera-

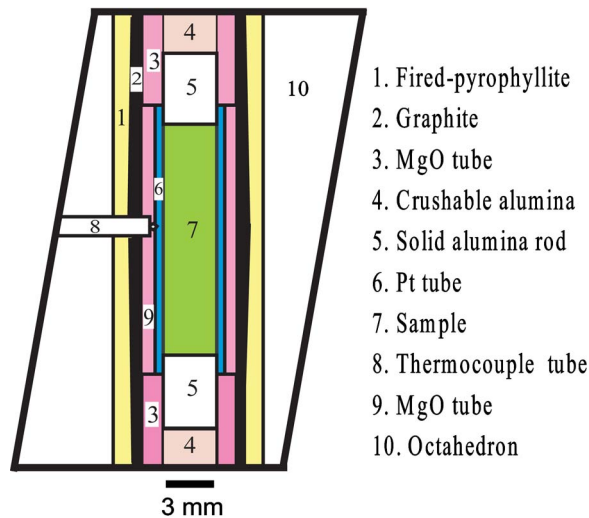


FIG. 3. (Color online) Cross section of sample assembly for the 18/11 truncations (Octahedron edge length / truncated edge length of WC cube).

ture of an ordinary piezoelectric transducer (PZT). We selected 36° *Y*-cut longitudinal lithium niobate (LiNbO_3) transducers that have a resonant frequency of 10 MHz to study the polarity of the first arrival *P* wave. These transducers have a Curie point of 1150°C , and a piezoelectric deformation constant of 8×10^9 V/m which is two to three orders of magnitude higher than that of an ordinary PZT. To improve the signal/noise ratio, signals from transducers are input into the amplifiers as soon as they come out of the multi-anvil box. They are then fed into the data sampling cards that contain a high-frequency analog-to-digital (A/D) converter and an on-board memory. The signals from all channels go through an OR gate that ensures any channel could be the trigger source while all channels remain strictly synchronized. The threshold voltage for triggering an event was set 100 mV in this study. Pretrigger memory is used in the system to make sure the onset wave form is properly recorded. The pretriggering works by recording all the signals in random access memory (RAM) for a short period and by removing them if there is no trigger. At each channel, the A/D converter has an adjustable sampling frequency up to 30 MHz and an amplitude resolution of 12 bits (1/4096).

The signal input range is adjustable at ± 50 mV ± 5 V. The digitized data are first stored temporarily in the on-board memory and then transferred to the computer memory in a circulating way so that there is no interruption of data sampling during the transfer. Saving the wave form data from computer memory into the hard disk takes about 0.4 s of dead time during which data sampling is not available.

C. Sample assembly

One of the major issues in studying high-pressure instabilities is the generation of nonhydrostatic stress. The ratio of sample length to diameter was adopted from Jung *et al.*⁷ to achieve nonhydrostatic stress for the instabilities. In our study, to generate nonhydrostatic stress under high-pressure and high-temperature conditions, we inserted a fully dense Al_2O_3 disk at the top and at the bottom of the specimen (Fig. 3). Three cell assemblies, with the octahedron edge length/

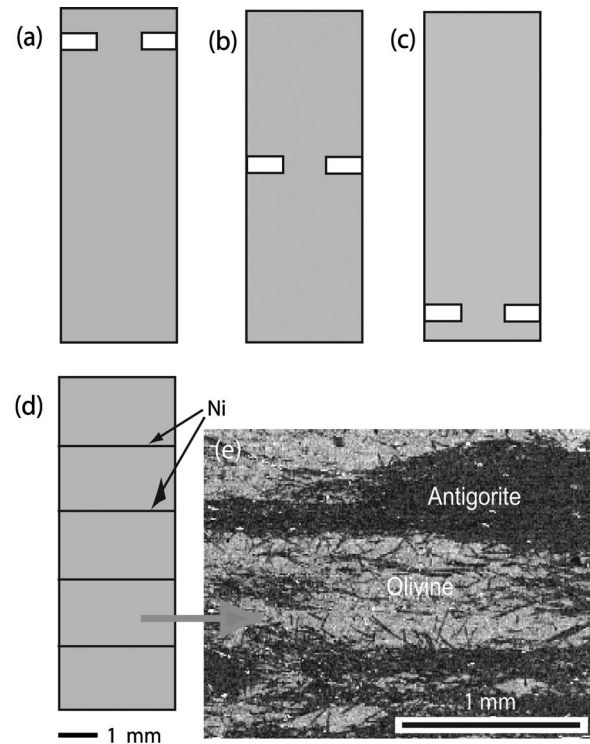


FIG. 4. Schematic drawings of starting materials which have a dimension of the length of 7.5 mm and the diameter of 3.1 mm. (a)–(c) Saw cut of WC rod. (d) Natural serpentinite sample with Ni evaporations to be used as a passive marker of a fault offset. (e) Backscattered electron images showing a typical microstructure of the natural serpentinite.

truncated edge length of tungsten carbide cube with 18/11, 10/5, and 8/3, respectively, could be used to achieve different pressures up to $P \sim 27$ GPa.¹⁹ The 18/11 cell assembly (Fig. 3), which could reach as high as 9 GPa, was used in the experiments described here. To minimize the temperature variation within the specimen caused by heat loss at the ends, we used a graphite furnace that had a thicker wall in the center and gradually tapered to a thinner wall at the ends.

III. HIGH-PRESSURE FAULTING EXPERIMENTS

A. Specimen

Sample materials used were WC rod and natural serpentinite from Val Malenco, Italy. The WC rods were used to constrain the source region of AE at various places within the sample and thereby to establish expected travel times, etc. The natural serpentinite was used to test our system at elevated temperature and its capability to detect, record, and characterize AE generated at high pressure and high temperature. The length and diameter of the specimens were 7.5 and 3.1 mm, respectively. We made a saw cut in the WC rod where it was to be broken during pressurization [Figs. 4(a)–4(c)]. Natural serpentinite disks were core drilled from the natural sample and Ni was evaporated on the surface of the disks. Assembly of experimental samples was achieved by stacking the disks. The presence of Ni at the interfaces between the disks provided a passive marker [Fig. 4(d)] that recorded fault offsets in each specimen for examination after that experiment. Figure 4(e) shows the starting material of the natural serpentinite that consists primarily of serpentine

TABLE I. Experimental conditions and results.

Run No.	Sample	P^a (GPa)	T^a (°C)	Number of AE ^b	P^c (GPa)	T^c (°C)
M520	WC center ^d	6	Rm T	52	1.3	Rm T
M521	WC top ^d	6	Rm T	50	0.3	Rm T
M526 ^e	WC bottom ^d	6	Rm T	16	0.3	Rm T
M527	WC top	3.3	Rm T	57	0.4	Rm T
M528	WC bottom	3.3	Rm T	57	0.4	Rm T
M529	WC center	3.3	Rm T	80	1	Rm T
M513 ^f	Serpentine	6	670	23	5	630 ^g
M514	Serpentine	6	860	25	6	770 ^g
M522 ^f	Serpentine	5.5	640	21	5.5	640 ^g

^aFinal pressure and temperature.

^bTotal numbers of acoustic emissions (AEs) detected during the experiment.

^cPressure and temperature at which tungsten carbide (WC) rod was broken and a sound was audible, and at which serpentine sample emitted acoustic signals at high pressure and high temperature.

^dWC center, -top, and -bottom refers to the tungsten carbide (WC) rod which was broken near the center, top, and bottom, respectively. Refer to the text for details.

^eTwo sensors took off at ~ 1.1 GPa.

^fExperimental procedures were different from others described in the text. Pressure of these runs was increased first up to 3.3 GPa in 1 h and temperature was raised to 550 °C in 30 min, followed by the simultaneous increase of both pressure and temperature to the target P/T conditions in ~ 7 min.

^gAn acoustic emission at the highest temperature of the run. There were several more acoustic emissions at lower pressure and temperature conditions from the specimen.

(antigorite) and relict olivine (remaining from the original rock that had not been fully converted to serpentine during natural alteration).

B. Experimental procedures

Pressure was increased first to the target pressure at a constant rate of 3.3 GPa/h. For the serpentine sample, temperature was raised at 20 °C/min to the maximum temperatures shown in Table I. Temperature was measured by W5 % Re/W26 % Re thermocouples with uncertainties less than ~ 20 °C due to the temperature gradient from the center to the ends of the specimen. Abundant electrical noise was detected when we used an AC power supply at the beginning of this project, but the electrical noise was eliminated later by using a DC power supply. During the experiments, wave forms of AE were recorded automatically on the four channels whenever there was an event triggered. At the target pressure and temperature, a specimen was quenched to room temperature in few seconds by shutting off the power of the heating system. Recovered specimens were analyzed using a Philips XL30-FEG scanning electron microscope (SEM).

C. Detecting acoustic emissions from the carbide experiments

We conducted nine experiments with the system (Table I). Specimens of the first six experiments were WC rod to constrain the source region of acoustic emission. In each of these experiments, the WC rod had grooves cut in one of three different locations: top, middle, and bottom [Figs. 4(a)–4(c)] to localize where failure would occur [subsequent examination showed that, as expected, the WC rods broke where they had been weakened by the groove; Figs. 5(a)–5(c)]. In each experiment, 50–80 AE events were recorded during pressurization up to ~ 2 GPa but they stopped

there even though pressurization continued up to 6 GPa. When the WC rod was broken, there was an audible sound accompanied with a large acoustic emission signal. The pressure at which the WC rod was broken is also shown in Table I.

Figure 6 shows an example of AE recordings from a sample in which the WC rod was broken close to the center. The positions of the first arrival were determined from a deviation which is larger than the amplitude of the background [Fig. 6(b)]. The travel time difference between the first and the last arrived signals was ~ 0.4 μ s. In contrast, Fig. 7 shows an example in which the WC rod was broken near the bottom. The arrival time on channel 4 was ~ 10 μ s earlier than those at the other channels. This observation shows that the arrival time difference between the first and the last arrived signal is ~ 10 μ s for the specimen of 7.5 mm long. Having the resolution of better than ~ 0.1 μ s in the wave form [Figs. 6(b) and 9(b)], we have a spatial resolution of ~ 75 μ m in the specimen. Subsequent examination of the recovered specimen revealed a macroshear crack near the

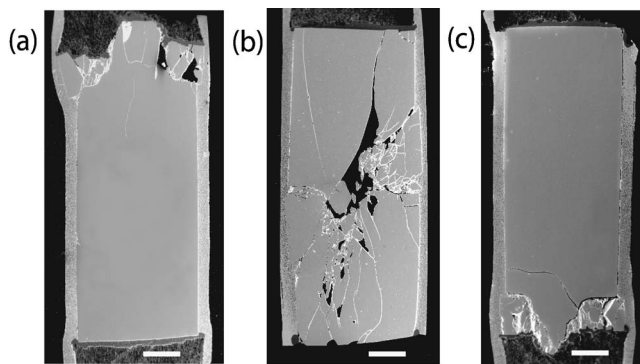


FIG. 5. (a)–(c) Backscattered electron images showing the broken carbide samples near the top, center, and bottom. Scale bars represent 1 mm.

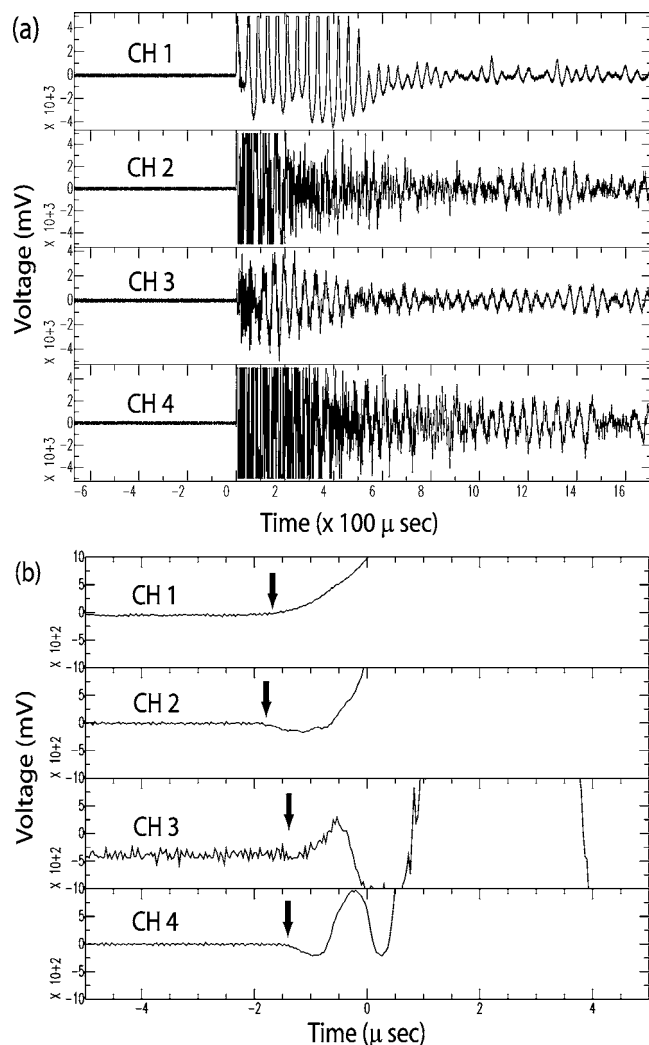


FIG. 6. (a) Acoustic signals with four channels of a shear event when a specimen, tungsten carbide rod, was broken near the center at $P=1$ GPa (M529). (b) Magnified view of (a). Please note that the polarity of the first arrival is different at different channels. Arrival time difference between the first and the last arrived signal is $\sim 0.4 \mu\text{s}$. Note also that the resolution in the wave form is better than $\sim 0.1 \mu\text{s}$.

bottom of the WC rod [Fig. 5(c)]. A simple calculation of the travel distance of waves between the position of transducers and the bottom of the WC rod gives that the travel distance of the transducer 4 from the bottom of the WC rod is about 7 mm shorter than those of the other three transducers. The reason why arrival times of the channels 1–3 are not the same is due to the fact that the cracks were not at the center of the WC rod bottom, but concentrated in one side. This first-degree approximation (assuming straight ray path) is consistent with the observed arrival times at different channels. Therefore, we can confidently associate this event with the observed macrocrack. This test also yields the more general conclusion that events occurring at either end of the sample could cause as much as $\sim 10 \mu\text{s}$ difference in arrival time at the different channels, which is also supported by the other three repeated experiments of the WC rods broken near the top and the bottom (Table I). Any events occurring within the sample should have an arrival time difference at different channels less than $\sim 10 \mu\text{s}$.

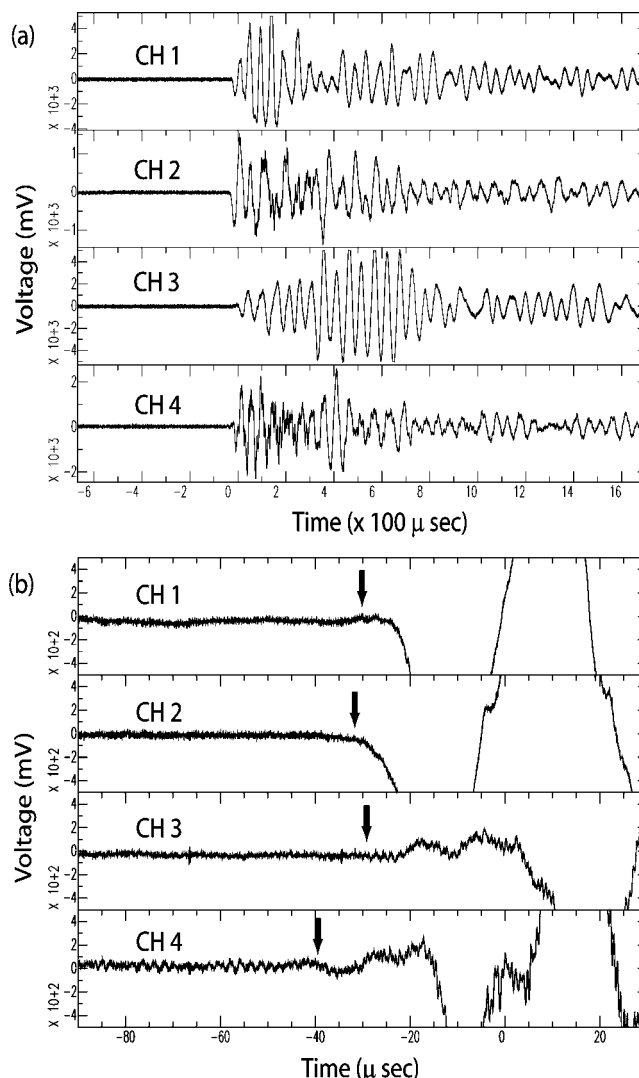


FIG. 7. (a) An example of acoustic emission with four channels when a tungsten carbide rod was broken near the bottom (M528). (b) Magnified view of (a). The arrival time at the channel 4 is $\sim 10 \mu\text{s}$ earlier than those at the other channels.

The wave form analyses after experiments showed that acoustic emissions could be divided into two categories. The first category is acoustic emissions that occurred outside the sample within the pressure medium (Figs. 3 and 8). These events are usually recorded only at one, two, or three of the four channels or at all four channels but with large differences in arrival times and amplitudes (Fig. 8). We interpret these events as microfractures in the anvils or collapse of the confining pressure media, or frictional slip between the anvils and the confining pressure media. The second category is the events that occurred in the sample. These events are recorded at all four channels with amplitudes of similar order and arrival times within $10 \mu\text{s}$ (Figs. 6 and 7) of each other. The polarity of the first arrival of most wave forms is clear. Therefore, events of shear, explosion, or implosion can be distinguished from each other.

D. Detecting acoustic emissions in serpentinite experiments

Three experiments of serpentinite were conducted to test the heating system of the apparatus. When we pressurized

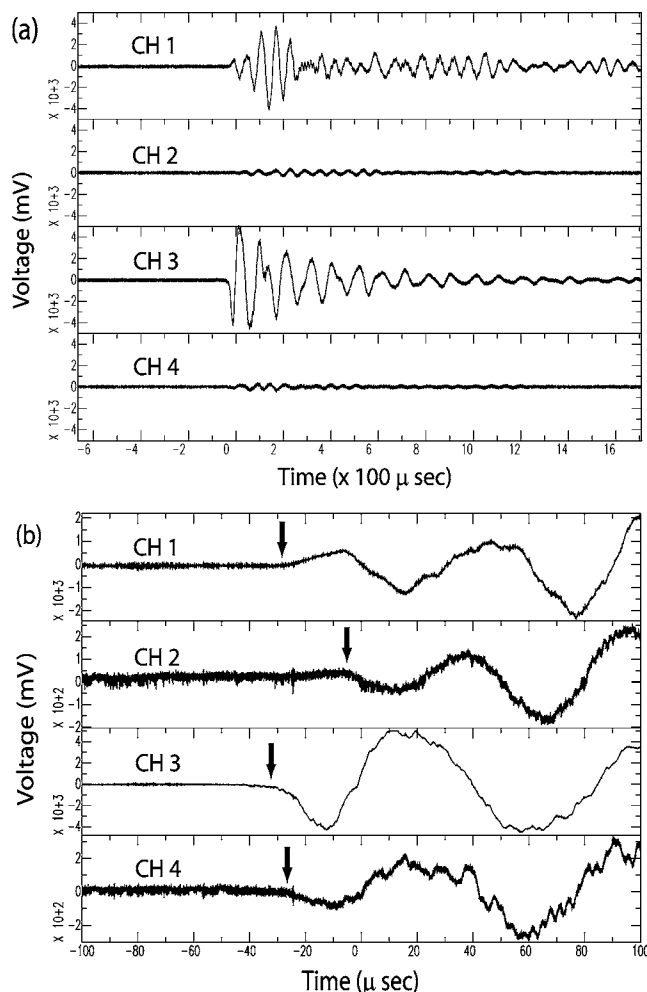


FIG. 8. (a) An example of acoustic emission occurred outside the sample area. Both channels 1 and 3 show a large amplitude whereas both channels 2 and 4 show a small amplitude. (b) Magnified view of (a). Please note that arrival time difference between the first and the last arrived signal is $\sim 30 \mu\text{s}$. This event may be caused due a frictional slip of the pressure media between the two anvils on which transducers 1 and 3 are attached.

the specimen (M514 in Table I) to 1 GPa, there were 17 acoustic emissions and one more acoustic emission at 5.2 GPa. During heating of the sample slowly to $T=860^\circ\text{C}$, there were seven more events. Acoustic emission was observed up to $P=6$ GPa and $T=770^\circ\text{C}$ is shown in Fig. 9(b). For this event, arrival time difference between the first and the last arrived signal was $\sim 0.5 \mu\text{s}$, indicating that the source of the acoustic emission was inside of the sample. This experiment shows that we can detect an acoustic emission under high-pressure and high-temperature conditions as high as $P=6$ GPa and $T=770^\circ\text{C}$ using the system.

IV. DISCUSSION

We have developed a four-channel system for detecting acoustic emissions in a multianvil apparatus. By conducting experiments using specimens of tungsten carbide (WC) rod, we have demonstrated that we are not only able to distinguish shear events from explosion, but also able to determine if the AE occurred within the sample or outside it. By conducting experiments on serpentinite, we have showed that the system can detect AE events high pressure up to at least

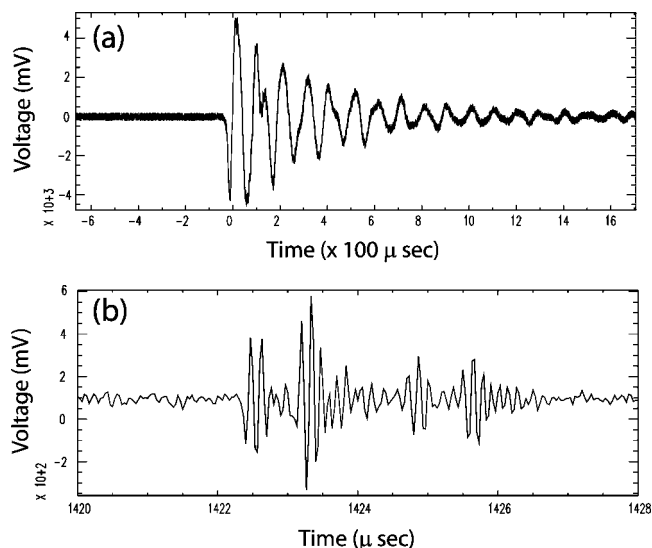


FIG. 9. (a) An example of acoustic emission at the pressure of 0.3 GPa and room temperature (M528) showing a low-frequency event. (b) An example of acoustic emission at the pressure of 3.3 GPa and at the temperature of 500°C (M513) showing a high-frequency event. The two plots show that the system resolves well the frequency range in about three orders (10 kHz–8 MHz).

6 GPa and at high temperature up to at least 860°C . Higher-pressure and temperature conditions can be reached up to the pressures of ~ 27 GPa and the temperatures of $\sim 2400^\circ\text{C}$ by using different sample assemblies and smaller truncations of tungsten carbide cubes. Therefore, this system can be very useful in searching for and in studying the characteristics of mechanical instabilities under high-pressure and high-temperature conditions.

The recorded wave forms showed that this system is sensitive to the events in a wide frequency band. The 30 MHz sampling rate puts an upper limit of 15 MHz for the frequency component recorded. Although the resonant frequency of the transducers is 10 MHz, its sensitivity remains large enough within the frequency band of 10 kHz–8 MHz (Fig. 9). The acoustic emissions reported by Meade and Jeanloz⁴ had a frequency of 1 MHz. Therefore, the frequency band covered by our system is large enough for an instability study at high pressure and high temperature.

The 0.4 s dead time was not a problem for detecting instabilities in the experiments on serpentinite because we did get acoustic signals during heating at high pressures. However, there is a potential risk that a noise event could occur right before (within 0.4 s) an instability takes place so that the signal caused by instability will be missed. Although the probability for this to happen seems very low, the dead time also prevents us from monitoring the cluster of instabilities should they occur. One way to circumvent this problem in our system would be to record continuously until the computer memory is full. Since the PC memory is large and the number of events at high pressure and high temperature is usually small, this is a practical solution for continuous recording for a small number (tens) of successive events.

We have shown that we can determine whether or not the event is beyond the top and bottom of the sample (Figs. 5 and 7). With the spatial resolution of $\sim 100 \mu\text{m}$ in the

system, we can also determine the location of an event beyond the side of sample by looking at travel time differences of the four channels ($>4 \mu\text{s}$) combined with an analysis of the microstructure of a postrun sample.

The experimental study of deep earthquakes requires multichannel wave form recording of acoustic emissions under high-pressure and high-temperature conditions. If a proposed mechanism of deep earthquake is to be valid, it must be able to cause shear radiation of the elastic energy. Event counting or single channel wave form recording used in previous studies were not capable of providing important information about the radiation pattern. Nor could such studies unambiguously distinguish real events from electronic noise, except in cases where coincidence of AE and stress drop could be correlated (e.g., Green *et al.*).³ Using the system, we have investigated the dehydration embrittlement of serpentine as a possible mechanism of intermediate-depth earthquakes. This work will be reported separately (Jung *et al.*).²⁰

ACKNOWLEDGMENTS

The authors thank Wenjie Jiao, Chris Hididiacos, Liqiang Liu, and Jin Ma for providing detailed technical information in designing the acoustic emission system. The authors also thank Baosheng Li for providing information on his interferometry and piezoelectric transducers. David Georges helped the authors to set up some of the hardware. One of the authors (H.J.) thanks G. Gudfinnsson and S. Keshav for useful discussions. We also thank Frank Forgit for sample assembly preparation. This project was supported

by the NSF Grant Nos. EAR-0125938, EAR-0135411 (H.W.G.), EAR-0125097 (Y.F.), and the Carnegie Institution of Washington.

- ¹H. W. Green and P. C. Burnley, *Nature (London)* **341**, 733 (1989).
- ²H. W. Green, T. E. Young, D. Walker, and C. H. Scholz, *Nature (London)* **348**, 720 (1990).
- ³H. W. Green, C. H. Scholz, T. N. Tingle, T. E. Young, and T. A. Koczyński, *Geophys. Res. Lett.* **19**, 789 (1992).
- ⁴C. Meade and R. Jeanloz, *Science* **252**, 68 (1991).
- ⁵D. P. Dobson, P. G. Meredith, and S. A. Boon, *Science* **298**, 1407 (2002).
- ⁶D. P. Dobson, P. G. Meredith, and S. A. Boon, *Phys. Earth Planet. Inter.* **143–44**, 337 (2004).
- ⁷H. Jung, H. W. Green, and L. F. Dobrzhinetskaya, *Nature (London)* **428**, 545 (2004).
- ⁸J. Zhang, H. W. Green, II, K. N. Bozhilov, and Z.-M. Jin, *Nature (London)* **428**, 633 (2004).
- ⁹H. Jung and H. W. Green, *Int. Geol. Rev.* **46**, 1089 (2004).
- ¹⁰D. A. Wiens, J. J. Mcguire, and P. J. Shore, *Nature (London)* **364**, 790 (1993).
- ¹¹D. A. Wiens, J. J. Mcguire, P. J. Shore, M. G. Bevis, K. Draunidalo, G. Prasad, and S. P. Helu, *Nature (London)* **372**, 540 (1994).
- ¹²P. G. Silver, S. L. Beck, T. C., Wallace, C. Meade, S. C. Myers, D. E. James, and R. Kuehnel, *Science* **268**, 69 (1995).
- ¹³W. Jiao, P. G. Silver, Y. Fei, and C. T. Prewitt, *J. Geophys. Res.* **105**, 28125 (2000).
- ¹⁴H. W. Green and C. Marone, *Rev. Mineral. Geochem.* **51**, 181 (2002).
- ¹⁵H. W. Green and H. Jung, *Elements*, **1**, 31 (2005).
- ¹⁶C. Meade and R. Jeanloz, *Nature (London)* **339**, 616 (1989).
- ¹⁷X. Lei, K. Kusunose, M. V. M. S. Rao, O. Nishizaqa, T. Satoh, *J. Geophys. Res.* **105**, 6127 (2000).
- ¹⁸X. Lei, K. Masuda, O. Nishizawa, L. Jouniaux, L. Liu, W. Ma, T. Satoh, and K. Kusunose, *J. Struct. Geol.* **26**, 247 (2004).
- ¹⁹C. M. Bertka and Y. Fei, *J. Geophys. Res.* **102**, 5251 (1997).
- ²⁰H. Jung, Y. Fei, P. G. Silver, and H. W. Green, *Nature (London)* (unpublished).